Investigating Performance of High-Rate GNSS-PPP and PPP-AR for Structural Health Monitoring – Dynamic Tests on Shaking table

Cemal Ozer Yigit[1,2], Ahmed El-Mowafy[3], Ahmet Anil Dindar[4], Mert Bezcioglu[5], Ibrahim Tiryakioglu[6]

[1] School of Earth and Planetary Sciences, Curtin University, Perth, WA, Australia. Email: cyigit@gtu.edu.tr

[2] Department of Geomatics Engineering, Gebze Technical University, Gebze, Turkey.

[3] School of Earth and Planetary Sciences, Curtin University, Perth, WA, Australia. Email: A.El-Mowafy@curtin.edu.au

[4] Department of Civil Engineering, Gebze Technical University, Gebze, Turkey. Email: adindar@gtu.edu.tr

[5] Department of Geomatics Engineering, Gebze Technical University, Gebze, Turkey. Email: mbezcioglu@gtu.edu.tr

[6] Department of Geomatics Engineering, Afyon Kocatepe University, Afyon, Turkey. Email: itiryakioglu@aku.edu.tr

ABSTRACT

This paper investigates the usability of the GNSS PPP methods, traditional PPP with a float-ambiguity solution and with Ambiguity Resolution (PPP-AR), in structural health monitoring applications based on experimental tests using a single-axis shaking table. To evaluate the performance of the PPP methodologies, harmonic oscillations of the motion table with amplitudes ranging from 5 mm to 20 mm and frequency between 0.2 Hz and 2.5 Hz were generated representing a wide range of possible structural motions. In addition, ground motion similar to those experienced during a real earthquake, the Kobe (1995), and step motions were generated on the shaking table. GNSS-PPP-derived positioning results were compared, in both of the frequency and time domains, with reference data comprising LVDT (Linear Variable Differential Transformer) data and relative positioning data. Results show that both PPP methods' measurements can be used in the computation of the harmonic oscillations' frequencies compared to the LVDT and relative positioning values. The observed amplitudes of the harmonic oscillations are slightly different from the LVDT values in the order of millimeters. Results of step motion experiment demonstrated that PPP-AR is better than traditional PPP in exhibiting the quasi-static or static displacement offsets. In addition, the capability of PPP-AR method is evaluated to the natural frequency of a small-scale structural model excited on the shaking table. The frequency spectrum of this small-scale structural model derived from the PPP-AR method is consistent with FEM (Finite Element Model) predicted value. All results demonstrate the potential of the high-rate GNSS PPP methods to reliably monitor structural and earthquake-induced vibration frequencies and amplitudes for both the structural and seismological applications.

Key words: PPP; High-rate GNSS; Structural Health Monitoring; Shaking table; Dynamic Properties

1. Introduction

High-rate GNSS positioning is a powerful method in monitoring dynamic displacement responses of man-made structures and surface wave motion caused by large earthquakes. Real-time and post-mission relative kinematic GNSS positioning methods that require a minimum of two GNSS receivers have been used to monitor dynamic displacements. Numerous studies have been carried out using such relative positioning methods to measure dynamic displacement responses of tall slender structures (Çelebi 2000; Li et al.2006; Breuer et al. 2008; Park et al. 2008; Yigit et al. 2010; Górski 2017), and long and short-span bridges (Roberts et al. 2004; Meng et al. 2007; Moschas and Stiros 2011; Xu et al. 2017). In addition, there have been a few experimental studies for evaluating the accuracy and precision of relative GNSS positioning methods for measuring dynamic displacement (Chan et al. 2006, Nickitopoulou et al. 2006; Psimoulis and Stiros 2008, Wang et al. 2011). The abilities of GNSS as seismometers and integration of GNSS with MEMS based accelerometers have been assessed based on shaking table tests in the past decade (Ge et al. 2000, Bilich et al. 2008; Bock et al. 2011, Shi et al. 2010; Hung and Rau 2013, Tu et al. 2013, 2014). However, relative GNSS methods used in these studies require the use of at least one nearby GNSS reference station located in a stable place.

In recent years, the GNSS Precise Point Positioning (PPP) method was developed (Zumberge et al. 1997; Kouba and Heroux 2001), and gained wide attention since it does not require the utilization of a reference station. The PPP technique is able to provide from centimeter- to decimeter-level accuracy based on the processing of un-differenced observations from a single GNSS receiver employing the orbital and clock corrections (El-Mowafy et al. 2017). High-rate GNSS PPP has been demonstrated to be an efficient absolute positioning method for crustal deformation monitoring (Savage et al.2004; Calais et al. 2006), GPS seismology (Kouba 2003; Avallone et al. 2011, Xu et al. 2013, Nie et al. 2016; Paziewski et al. 2018; Xu et al. 2019), earthquake early warning system (Li et al. 2013) and structural health monitoring (Moschas et al. 2014; Yigit 2016; Yigit and Gurlek 2017; Tang et al. 2017; Kaloop et al. 2018).

The real-time PPP method, which needs real-time reception of the corrections, is suitable for natural hazard early warning systems. However, assessing the health condition of any engineering structures after a natural event is crucial and necessary to prevent future disasters and for saving lives. Therefore, post-process GNSS-PPP is also required to obtain the precise and accurate displacement history of structures, since its accuracy is typically better than real-time GNSS-PPP. In addition, post-process GNSS-PPP is also needed when real-time products (RTS) are not feasible, for instance, due to loss of internet service, needed to access the RTS web server, that my happen after an earthquake.

This contribution evaluates the performance of both traditional post-process PPP and PPP-AR methods for measuring the dynamic and quasi-static displacements of man-made structures under dynamic loadings, such as wind, earthquake loading, etc. The research investigates how precisely can GNSS-PPP measure these movements, and demonstrates the potential of PPP as an alternative approach to relative positioning in case there is no base station available on site or usable due to strong ground motions, or the accuracy of its known location may be changed as a result of the earthquake. The evaluation of the performance of high-rate PPP method was carried out on harmonic oscillation events, a simulation of the Kobe earthquake, and step motion for quasi-static deformation generated by a single-axis shaking table with a mounted GNSS antenna and LVDT sensor. The PPP results obtained from each experiment were compared to the corresponding LVDT data and relative GNSS positioning in the time and frequency domains. Furthermore, the PPP-AR method was tested on the small-scale model

excited by the shaking table. Natural frequencies of the small-scale model derived from the PPP-AR method are compared to the Finite Element Mathematical Model (FEM) results. The FEM model is the mathematical representation of the small-scale test model and was updated in an earlier research project. The presented results are not only relevant to structural monitoring applications but are also important for seismology.

This paper is organized as follows: The traditional PPP and Ambiguity-fixed PPP models are briefly presented in Section 2. The experimental setup utilized in this research is explained in Section 3. In section 4, GNSS data processing is briefly given. The test results are discussed in Section 5. Finally, the conclusions are given in Section 6.

2. Precise Point Positioning methods

In this study, high-rate GNSS data were processed by both traditional PPP and PPP-AR methods to explore the strengths and weaknesses of each method. The fundamental mathematical background of these approaches is briefly overviewed in this section.

2.1 Traditional PPP

The traditional ambiguity-float PPP usually utilizes ionosphere-free (IF) combinations along with satellite clock corrections to the broadcast clock corrections, and precise orbits in post-mission or orbit corrections to broadcast orbits in real-time processing. The observation equations for pseudorange code and carrier phase measurements for satellite s on frequency i in length units can be expressed as (El-Mowafy et al. 2016):

$$P_{IF}^s + c\,\widetilde{dt}^s = \rho^s + c\,\widetilde{dt}_r + T^s + \varepsilon_{P_{IF}^s} \tag{1}$$

$$\phi_{IF}^s + c\,\widetilde{dt}^s = \rho^s + c\,\widetilde{dt}_r + T^s + \lambda_{IF}\,\widetilde{N}_{IF}^s + \varepsilon_{\phi_{IF}^s} \tag{2}$$

and the biased (real-numbered-float) ambiguity term $(\lambda_{IF}\,\widetilde{N}_{IF}^s)$ is expressed as:

$$\lambda_{IF}\,\widetilde{N}_{IF}^s = [(A\,\lambda_1\,N_1^s - B\,\lambda_2\,N_2^s) + (A\,\delta_{r,1}^s - B\,\delta_{r,2}^s) + (A\,d_1^s - B\,d_2^s) - (A\,d_{r,1} - B\,d_{r,2})] \tag{3}$$

where P_{IF}^s and ϕ_{IF}^s are the ionosphere-free code and carrier-phase observations, respectively; ρ^s is the satellite-to-receiver geometric range; c is the speed of light in vacuum. It is assumed here that the IGS products for L1 and L2 GPS observations are used, such that the biased ionosphere-free combination satellite clock offset $c\,\widetilde{dt}^s$ includes the satellite code biases (d_1^s and d_2^s), such that $c\,\widetilde{dt}^s = c\,dt^s + (A\,d_1^s - B\,d_2^s)$, where $c\,dt^s$ is the original satellite clock offset, $A = \frac{f_1^2}{f_1^2 - f_2^2}$ and $B = \frac{f_2^2}{f_1^2 - f_2^2}$; Similarly, the biased ionosphere-free combination receiver clock offset $c\,\widetilde{dt}_r$ used for both code and phase observations includes the receiver code biases ($d_{r,1}$ and $d_{r,2}$), such that $c\,\widetilde{dt}_r = c\,dt_r + (A\,d_{r,1} - B\,d_{r,2})$, where $c\,dt_r$ is the unknown receiver clock offset; $\delta_{r,1}^s$ and $\delta_{r,2}^s$ are the combined satellite and receiver phase biases; λ_1 and λ_2 are the wave lengths for L1 and L2. T^s is the troposphere delay. It is assumed that the receiver hardware biases are the same for measurements of the same frequency for all

satellites from the same constellation. Typically, phase delays like phase windup, antenna offset, relativistic errors are estimated from empirical models and are reduced from the phase observations before being used. Finally, $\varepsilon_{P_{IF}^s}$ and $\varepsilon_{\phi_{IF}^s}$ are the ionosphere-free code and carrier-phase observation noise.

In this model, the float ambiguity term $(\lambda_{IF}\,\widetilde{N}_{IF}^s)$ is estimated as part of the unknowns every epoch. To avoid rank-defect of the model, code observations are needed. Because of the high noise of code observations and the slow variation of the satellite geometry over time the ambiguity values need approximately 30 minutes or more (depending on satellite number and geometry) to stabilize and to converge the solution to the decimeter level of accuracy.

2.2 PPP with ambiguity resolution (PPP-AR)

Traditional PPP has involved the use of ambiguity float solutions which require long observation time to converge to centimeter accuracy. The purpose of PPP with ambiguity resolved (PPP-AR) is to shorten the solution convergence time and to improve positioning accuracy. As shown in (3), the integer carrier-phase ambiguities are mixed with the code and phase biases, therefore, to capture the integer property of the ambiguities, these biases should be accounted for. Hence, the generic Radio Technical Commission for Maritime Services (RTCM) standard is to transmit both the code and phase biases. However, this is not necessarily needed if no ionosphere corrections are transmitted to the user.

Several PPP-AR methods have been developed in the past decade. Ge et al. (2008) presented a between-satellites approach that eliminates receiver biases through a single-differencing of the observations. The integer property of the ambiguities is recovered by sequentially correcting the satellite wide-lane and narrow-lane fractional-cycle biases. Collins et al. (2010) developed a method known as the decoupled clock model including that the code biases into the fractional part of phase ambiguities. By applying the satellite decoupled clock corrections (i.e. clock corrections for code observations that are different from the clock corrections of the phase observations) and computing the receiver decoupled clock parameters, both the undifferenced integer wide-lane ($N_1^s - N_2^s$) and N_1^s ambiguities can be directly estimated. Another method is developed by Laurichesse et al. (2008) which similarly included the use of different clock terms for code and carrier-phase observations. The method uses the wide-lane satellite bias corrections to estimate the integer wide-lane ambiguity, and thus the integer N1 ambiguity is directly estimated. For more details, the interested reader can refer to the given references. Nevertheless, it should be noted here that the user should apply a method consistent with the method used for computation of the corrections by the provider, that is typically estimated by employing measurements from a network of reference stations.

3. Experimental setup

3.1 Shaking table

Shaking table is an electro-mechanical system that simulates the harmonic or random motions of the observation point. Fundamentally, the shaking table is composed of a reference table where the motion is created, a controller unit that defines the amplitude of the motion, and a motion table that moves in uniaxial- or biaxial-directions. The shaking table used in the

experiments of this study can move the motion table, shown in Fig. 1 as the black flat plate where the receiver is attached, in a uniaxial direction within ± 95 mm. The total stroke of the table is 190 mm. The table follows either displacement or an acceleration pattern, with harmonic motions or single steps. The maximum velocity is limited to 400 mm/s. The motion of the table is provided by an electric engine that creates negligible vibrations. The stability of the table on a metal chassis under high frequency motions are maintained by counter-weights placed on the two sides of the platform. The position of the table on the rails is controlled by software running on a Windows laptop where the controller verifies the position using an embedded LVDT under the motion table (not visible in Fig. 1). The LVDT measures the position of the table at mm level accuracy with 50 sps (sampling per second), i.e. 50 Hz.

The motion patterns of the shaking table can be arranged as harmonic and random values. The harmonic motions are a function of a sinusoidal wave that is described by the amplitude, frequency and number of cycles. On the other hand, random values are described as acceleration or displacement values. The acceleration values are initially converted to the displacement in order to see whether the peak values exceed the stroke limits. In case of exceeding the stroke limit, the time-history values are linearly scaled by an optimal factor for the sake of consistency between the peak to peak scaled values and the stroke limits.


Fig. 1. Shaking table

3.2 Small-scale model structure

The system tested on the shaking table is a small-scale model structure that behaves as a shear-type building. The model produced and validated as a benchmark specimen in a previous research project (Akpınar et al, 2017) is composed of steel columns and aluminum plates. There are three stories with 50 cm in height and the columns connected to the plates. The total height and the weight of the model structure is 150 cm and 21.2 kgf, excluding the GNSS receivers. During the motions, the chassis under the shake-table is about 75kgf in weight and it is believed that a counter-mass is maintained adequately. The model structure has specially designed rectangular aluminum connection plates, shown in Fig. 2(a), used to limit the out-of-plane movement. The natural behavior of the model structure is a transition into the principal axis; the first transition mode is towards where the connection plates are weakly oriented, and the second transition mode is towards the strong direction of the plates. Following the transition modes, the rotation mode takes place. The numerical vibration frequencies calculated through the Finite Element Model analysis are 3.33 Hz, 4.65 Hz and 4.73 Hz for the first three modes,

respectively, as seen in Fig. 2 (b-d). The masses of the tribrach and GNSS receivers on top of the model were included in the FE analysis.
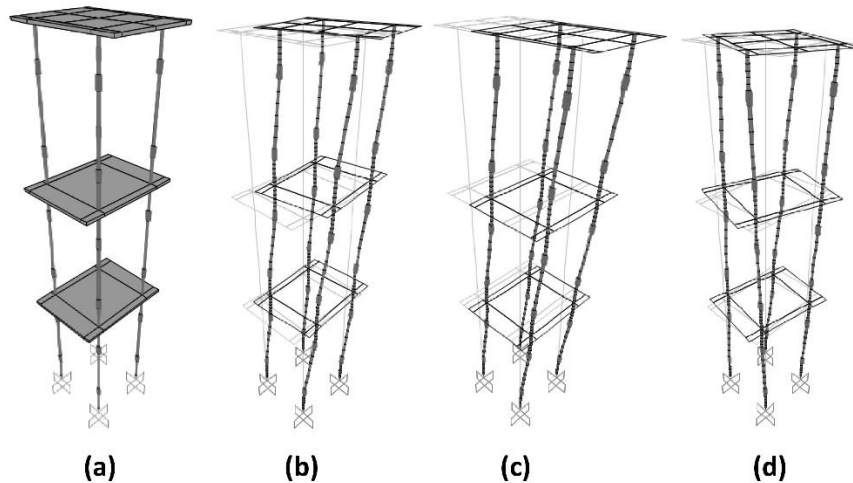
Fig. 2. Finite Element Model of the Structure, (a): perspective, (b-d): 1st, 2nd and 3rd modes.

The small-scale model in this study has behaved in the elastic region through all tests, no plastic deformation has been observed from the structural members (columns, connection plates etc.). This observation was confirmed with the hammer test results. The hammer test is a simple impulsive force acted on the structure to obtain the response from a wide range of frequencies and conducted after the motion tests.

3.3 GNSS data collection

In this study, we employed two GNSS receivers, which are dual frequency Topcon™ HiPer-Pro. One GNSS receiver was mounted on the shaking table (cf. Fig. 1). Another GNSS receiver was installed 20 m away from the shaking table at a known station and served as a reference station. The shaking table experiments, including harmonic, ground and step motions, were conducted at the Istanbul Kültür University campus in Istanbul in August 2016 and lasted approximately 136 minutes. The shaking table was kept immobile for approximately 25 minutes before starting the harmonic oscillation test for accelerating the process of achieving an integer ambiguity-fixed for relative positioning and PPP-AR and a stable float-ambiguity solution for traditional PPP (hereafter referred to simply as PPP), respectively. The GNSS observations were recorded at a 10 Hz sampling rate. Both GPS and GLONASS satellite data were collected. The number of observed GPS+GLONASS satellites varied between 12 and 16 per epoch during the experiment. The experiment was conducted under open-sky conditions and with calm weather.

3.4 Description of the experiments

3.4.1 Harmonic oscillation experiments

A large set of different harmonic oscillation experiments using a shaking table have been conducted to evaluate the performance of the high-rate PPP methods and to compare their

results with a reference LVDT data and GNSS relative positioning. To cover a wide range of structural motions, 'Sine' oscillations with amplitudes from 5 mm to 20 mm and frequency between 0.2 Hz and 2.5 Hz were generated for the dynamic motions. Table 1 summarizes selected harmonic oscillation events generated by the shaking table during the experiments, giving their frequency and amplitude values.

Table 1. Selected frequencies and amplitudes of the sinus wave oscillations generated by the shaking table

Frequency	0.2 Hz	0.5 Hz	1 Hz	1.5 Hz	2 Hz	2.5 Hz
Amplitude	5 mm	5 mm	5 mm	5 mm	5 mm	5 mm
	10 mm	10 mm	10 mm	10 mm	10 mm	10 mm
	15 mm	15 mm				
	20 mm	20 mm				

3.4.2 Earthquake simulation experiment

Kobe earthquake, also known as the Great Hanshin earthquake, occurred on January 16, 1995, at 20:46 UTC in the southern part of Hyōgo Prefecture, Japan. The earthquake had a moment magnitude (Mw) of 6.9. In this study, the random values representing strong ground motion is excerpted from a natural wave form recorded in Kakogawa-KKGW station during the Kobe earthquake. The epicentral distance to the recording station was about 20 km. The recording has near-field characteristics of high-amplitude and short duration (~20 seconds). The displacement computed from the acceleration data was scaled down (0.35 times) in order to be within the stroke limits of the shaking table.

3.4.3 Step motion (displacement offset) experiment

Following the harmonic tests, the quasi-static displacement offset tests were performed in order to compare the performance of PPP and PPP-AR. The quasi-static test displacement protocol was chosen as 1 cm increment of the position of the motion table after every 60 seconds. The velocity of the applied increment was very slow in order not to create any oscillation of the model structure. The quasi-static displacement offset tests were motivated from the fact that the long-period engineering structures namely high-rise buildings, dams, and bridges are vulnerable to slow but continuous actions. These actions may comprise the constant wind loading, change of the soil conditions, poor design or poor construction of the pile foundations after long-term settlement. Those cases represent indeed a quasi-static change of the position of the structures which cannot be observed by dynamic measurement units.

3.4.4 Small-scale model experiment

The small-scale model explained in section 3.2 represents a shear-type frame system that can be laterally excited on the shake-table under harmonic functions with different amplitudes and frequencies. The small-scale model has special deformation plates at the tips of the columns to prevent the nonlinear rotations and out-of-plane motions of the entire structure. The fundamental vibration periods of the model structure were computed by a Finite Element Mathematical Model (FEM) and compared with the position variation determined by PPP-AR.

Since the structure is symmetrical in geometry, the first mode is expected to be a transition rather than a rotation mode. The response of the model was measured by the two GNSS receivers placed on top. The receivers were placed on either side of the top floor aligned in a direction perpendicular to the movement axis. The transition mode is expected to cause the dominant response, as one of the receivers was mounted on a tribrach instead of being mounted directly on the plate (GNSS2 in Fig. 3). The purpose of this addition is to provide more mass for controlled rotation. The open-sky experiments were conducted at Gebze Technical University campus in September 2017. The sampling rate of the both GNSS receivers was 10 Hz.
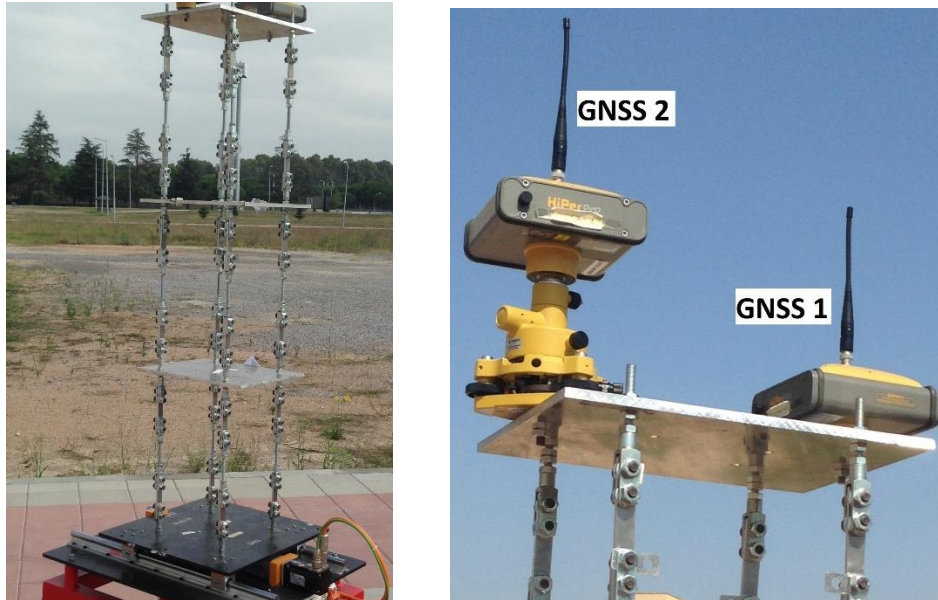
Fig. 3. Small-Scale Model on shaking table (Left) and GNSS receivers on top of the small-scale model (Right)

To determine the dynamic characteristics, the best practice is applying an impulse force to the specimen. The impulse force (in this study named as hammer test) creates a broad band response with the exception of the natural frequency value where the resonance occurs. Following the harmonic motions tests, the small-scale system waited for the static equilibrium. Then, an impulsive force by a hammer was applied to the small-scale structure. Since the exciting force is applied in a very short duration, the response is a pure free-vibration phase where the natural vibration frequency can be computed from the motion measurements.

4. DATA PROCESSING

4.1 Kinematic relative positioning processing

The GNSS relative positioning data was processed using the Leica Geo Office (LGO) 3.0 software. GNSS integer ambiguity-fixed solution was computed. The broadcast ephemeris was used for the post-processed kinematic solution.

4.2 Kinematic GNSS-PPP processing

The rover GNSS data on the shaking table were processed in the post-mission kinematic PPP mode using the old and modernized version of CSRS-PPP software developed by the NRCan-GSD (Geodetic Survey Division of the Natural Resource Canada). It is able to compute stand-alone positions from both single- and dual-frequency multi-constellation satellite data. In August 2018, the old online CSRS-PPP generated float-ambiguity PPP solution tool, switched to a modernized tool, which fully supports multi-GNSS data, and generates ambiguity resolved PPP (PPP-AR) solutions, and move towards faster convergence times (https://webapp.geod.nrcan.gc.ca/geod/tools-outils/documentation.php). The CSRS-PPP is capable of processing data sampled at 1 Hz and higher. CSRS-PPP software uses different GNSS orbit and clock products (ultra-rapid, rapid and IGS-Final) depending on the time of a user's data submission and the epoch of the last observation in users' dataset (Mireault et al. 2008). In this study, the IGS-Final precise orbit and clock products were used. Alternatively, one can use real-time products from the IGS online service or commercial providers (El-Mowafy et al. 2017; El-Mowafy 2018). The reader is referred to (Tétreault et al. 2005) for further details about the software.

4.3 Preliminary data processing (3D and 2D coordinate transformation)

Geocentric Cartesian coordinates or ellipsoidal coordinates cannot be directly used in structural health monitoring (SHM) or seismological applications (Yigit 2016), and therefore need to be transformed to a local topocentric Cartesian coordinate system. The geometric relation between these coordinate frames is illustrated in Fig. 4. Afterwards, topocentric coordinates should be projected onto the movement direction of the shaking table in order to obtain real movements of the shaking table and to be compared with LVDT data, which measures only one direction movement, as illustrated in Fig. 5.
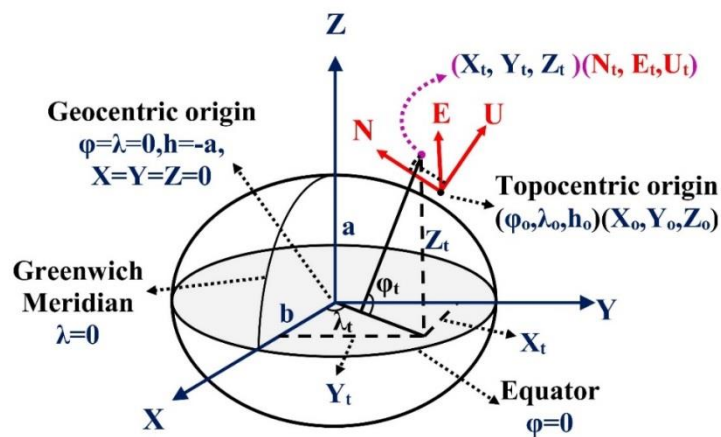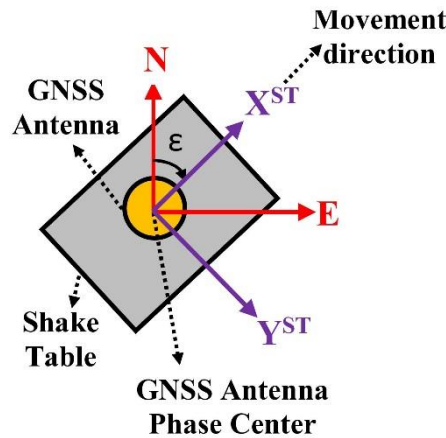

Fig. 4. Geocentric and Topocentric Coordinate Systems

The geocentric coordinates of a point (X_t, Y_t, Z_t) at time t can be converted into topocentric Easting, Northing and Up coordinates (E_t, N_t, U_t) by using the Euler transformation as follows:

$$\begin{bmatrix} E_t \\ N_t \\ U_t \end{bmatrix} = \begin{bmatrix} -\sin(\lambda_0) & \cos(\lambda_0) & 0 \\ -\sin(\varphi_0).\cos(\lambda_0) & -\sin(\varphi_0).\sin(\lambda_0) & \cos(\varphi_0) \\ \cos(\varphi_0).\cos(\lambda_0) & \cos(\varphi_0).\sin(\lambda_0) & \sin(\varphi_0) \end{bmatrix} \times \begin{bmatrix} X_t - X_0 \\ Y_t - Y_0 \\ Z_t - Z_0 \end{bmatrix} \qquad (4)$$

where (X_0, Y_0, Z_0) and (φ_0, λ_0) are the geocentric and ellipsoidal coordinates of the topocentric origin of the coordinate frames, respectively.

**Fig. 5.** Topocentric Coordinate and Shaking table Coordinate axis

Next, the topocentric (N, E) coordinates are projected onto the movement direction of the shaking table in its local coordinate system (X^{ST}, Y^{ST}) (cf. Fig. 5), such that:

$$\begin{bmatrix} X^{ST} \\ Y^{ST} \end{bmatrix} = \begin{bmatrix} \sin(\varepsilon) & \cos(\varepsilon) \\ \cos(\varepsilon) & -\sin(\varepsilon) \end{bmatrix} \times \begin{bmatrix} E \\ N \end{bmatrix} \tag{5}$$

where ε is the rotation angle between two coordinate systems (e.g. N and X^{ST} axes) as illustrated in Fig. 4. The X^{ST} axis coincideds with the movement direction representing the signal. The Y^{ST} axis, perpendicular to the X^{ST} axis, representing the GNSS' noise (Psimoulis and Stiros 2008) since the movement is in one direction.

5. Results and discussions

In this section, results of harmonic motions with various combinations of oscillation characteristics, a simulation of a real earthquake (Kobe earthquake), step motion experiment and small-scale model experiment, respectively. For the first three experiments, LVDT data and relative GNSS positioning solutions are considered as a reference to evaluate the performance of the high-rate PPP and PPP-AR methods. Fig. 6 illustrates the derived displacement time series for the two types of motion consecutively, namely harmonic oscillations and step motion. The time series from top to bottom refer to results of LVDT, relative positioning, PPP and PPP-AR. The latter two are obtained after solution convergence. It can be clearly seen that LVDT and relative positioning-derived displacement are very much consistent, whereas the PPP-derived displacement exhibits additional low frequency (long period) fluctuation. Compared with PPP, PPP-AR derived displacement, especially for a long period of time, is generally more consistent and better follows the relative positioning derived displacement.
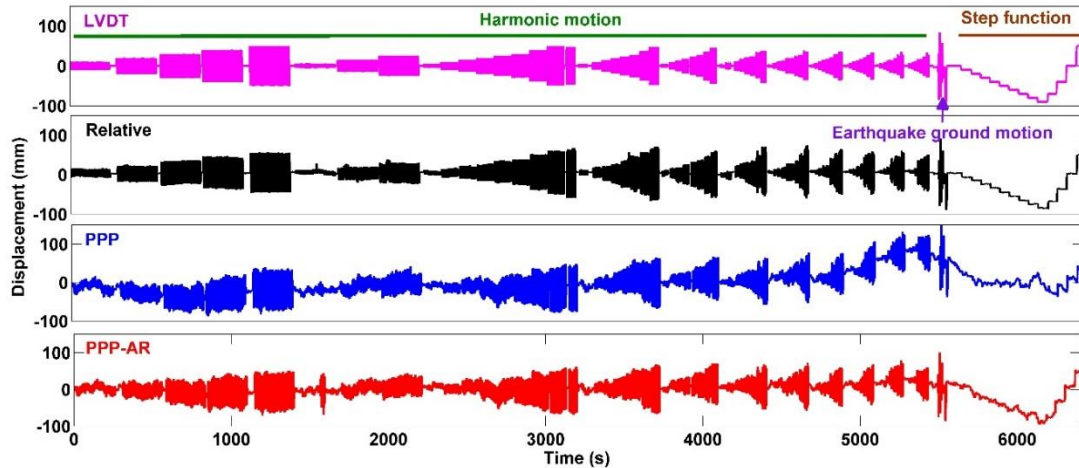
Fig. 6. Overall LVDT, Relative GNSS positioning, PPP and PPP-AR-derived displacement.

In order to further illustrate the positioning performance of the PPP and PPP-AR techniques for a long period of time, Fig. 7 shows the time series and distribution of the differences between those two methods and the relative positioning method. The top panel shows the time series of the differences, and the bottom panel shows histograms of the differences for PPP differences (left subfigure), and for PPP-AR differences (right subfigure.). It can be seen that PPP-AR is more consistent, and its differences range from – 2 cm to 2 cm and follow a Gaussian error distribution. On the other hand, PPP differences range from -5.5 cm to 8 cm and do not follow a Gaussian error distribution. The larger variation in PPP-derived displacement time series is due to the use of float-ambiguities, where more variation in the solution accuracy result from the small changes in the float values of the ambiguities and a long time is needed for reaching a converged solution. The convergence time represents the time to reach a stable accuracy level, depending on many factors such as observation quality (particularly the noise level of code observations), user environment, the number and geometry of visible satellites, sampling rate and algorithm (Bisnath and Gao 2008). However, the long-term fluctuation is not an issue if it is focused on the dynamic displacement over a short period of time, e.g., within 20 s to 250 s. The long-period fluctuation in PPP-derived displacement time series can be eliminated by implementing a high-pass filter (Yigit 2016). A more in-depth analysis of results of the four test cases (harmonic oscillations, Kobe earthquake simulation, step motion and small-scale structure model) will be given in the following four subsections.
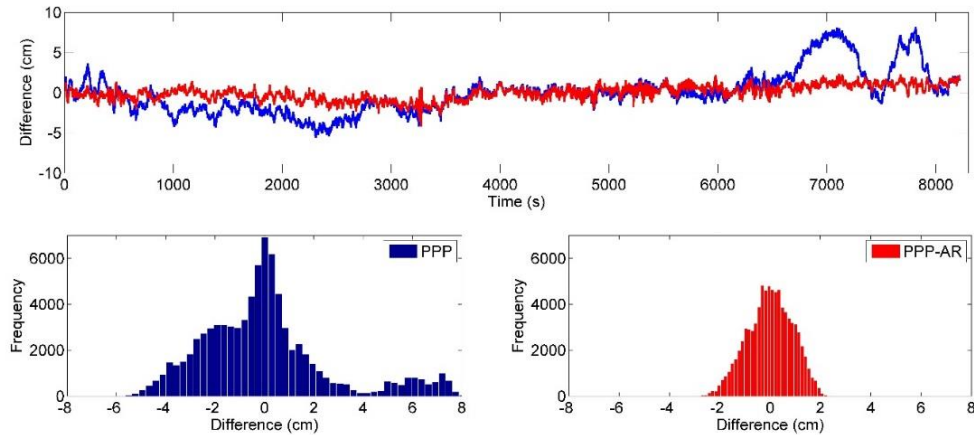
Fig. 7. Time series and histogram of displacement differences of PPP and PPP-AR from relative positioning

5.1 Results of harmonic oscillation tests

In this study, the offset and local trend component for each harmonic event selected were independently removed from PPP-derived time series. Fig. 8 shows the LVDT, relative GNSS positioning, PPP and PPP-AR derived displacement time series and the FFT (Fast Fourier Transform) spectrums of a representative event selected for comparing the methods (1 Hz frequency with 10 mm of amplitude). It can be seen in Fig. 8 that both PPP and PPP-AR-derived displacement show good agreement with that of the LVDT and relative-GNSS derived displacement. However, both PPP and PPP-AR have some low frequency component other than the given frequency during the shown 50 seconds. In addition, the oscillation frequencies obtained from all methods for this event are the same, whereas there are slight differences in the corresponding amplitudes. The differences and low frequency component shown for PPP and PPP-AR results can be attributed to multipath, random noise of carrier phase and higher order ionospheric errors (Shu et al. 2017).
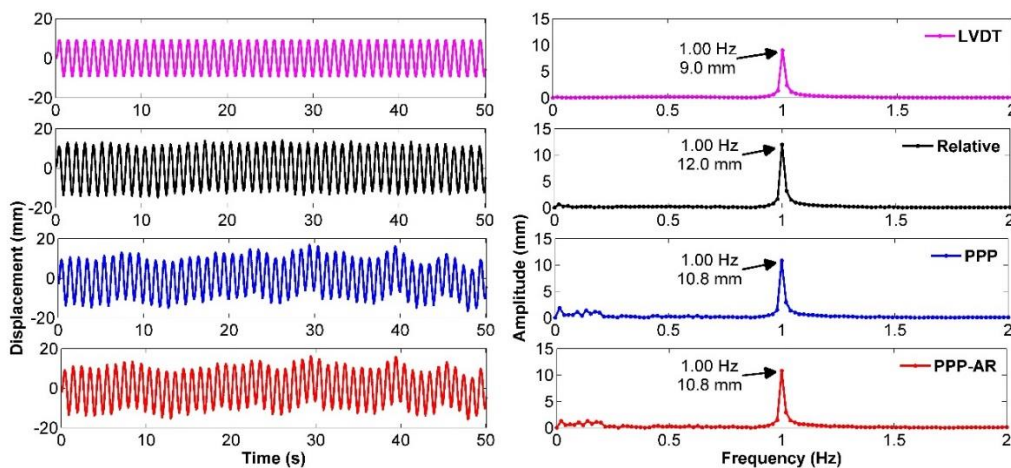
Fig. 8. Displacement time series and FFT spectrum of LVDT, Relative GNSS positioning, PPP and PPP-AR for a given 1 Hz frequency with 10 mm of amplitude

In post-mission processing, the low frequency component appeared in PPP and PPP-AR could be filtered out by applying a high-pass or a band-pass filter to extract the signal describing the dynamic displacements. However, in this study, high-pass or band-pass filters were not implemented to give a representative comparison, and only offsets and local trends for each event were independently removed from PPP-derived displacement time series.

To further examine the ability and performance of a high-rate PPP processing, the peak frequency and corresponding amplitude of each event obtained from FFT are summarized in Table 2. In addition, figure 9 demonstrates the amplitude of peak frequency obtained from FFT for given 5- and 10-mm amplitude to make the comparison easy. As can be seen from the table, the oscillation frequencies determined by LVDT, relative positioning, PPP and PPP-AR perfectly match for all events. However, there are slight differences in the corresponding amplitudes (Fig. 9). The differences in the amplitude of the oscillation frequency between the LVDT and PPP or PPP-AR vary between 0.1 mm and 1.8 mm. The differences in the amplitude of the oscillation frequency between relative GNSS positioning and PPP-AR vary between 0.0 and 1.2 mm, whilst the differences between relative positioning and PPP are from 0.0 to 1.5 mm, as shown in Table 2. As can be seen from figure 9, the differences in the amplitude of the oscillation frequency between all methods are small at low oscillation frequencies, on the other hand, the differences are slightly larger at high oscillation frequencies. These differences are mainly due to inherent GNSS noise and multipath. Overall, the harmonic oscillation tests demonstrate that the PPP and PPP-AR methods are good potential methods in determining the natural frequencies of engineering structures in case where the reference GNSS station data is unavailable or unreliable for RTK (real-time kinematic) relative GNSS positioning (where a base station would be needed) in the case of large (mega) earthquake.

Table 2. Peak Frequency and amplitude for all events using different methods.

Excitation Parameters	LVDT	Relative GNSS Positioning	PPP	PPP-AR
Frequency [Hz] (Amplitude [mm])				
0.20 (5.0)	0.20 (5.0)	0.20 (4.8)	0.20 (4.7)	0.20 (4.4)
0.20 (10.0)	0.20 (9.8)	0.20 (9.7)	0.20 (9.9)	0.20 (10.0)
0.20 (15.0)	0.20 (14.9)	0.20 (15.5)	0.20 (15.6)	0.20 (15.5)
0.20 (20.0)	0.20 (19.8)	0.20 (19.5)	0.20 (19.5)	0.20 (19.5)
0.50 (5.0)	0.50 (4.7)	0.50 (4.8)	0.50 (4.9)	0.50 (5.0)
0.50 (10.0)	0.50 (9.3)	0.50 (9.7)	0.50 (9.9)	0.50 (9.9)
0.50 (15.0)	0.50 (14.0)	0.50 (14.6)	0.50 (14.8)	0.50 (14.8)
0.50 (20.0)	0.50 (18.7)	0.50 (19.4)	0.50 (20.0)	0.50 (20.0)
1.00 (5.0)	1.00 (4.5)	1.00 (6.1)	1.00 (5.6)	1.00 (5.7)
1.00 (10.0)	1.00 (9.0)	1.00 (12.0)	1.00 (10.8)	1.00 (10.8)
1.50 (5.0)	1.51 (4.4)	1.51 (6.2)	1.51 (5.6)	1.51 (5.7)
1.50 (10.0)	1.51 (8.7)	1.51 (11.5)	1.51 (10.0)	1.51 (10.3)
2.00 (5.0)	2.01 (4.0)	2.01 (4.3)	2.01 (3.7)	2.01 (3.8)
2.00 (10.0)	2.01 (8.0)	2.00 (9.1)	2.00 (7.8)	2.00 (7.9)
2.50 (5.0)	2.52 (4.0)	2.52 (4.1)	2.52 (3.5)	2.52 (3.6)
2.50 (10.0)	2.52 (7.9)	2.52 (7.4)	2.52 (6.3)	2.52 (6.6)

The obtained displacement values in Table 2 are within the limits of the engineering structures' response during the seismic and wind actions. For the low- and mid-rise buildings, the seismic actions create the lateral drift motions at 2% of the building height whereas for the high-rise

buildings, not only seismic but also wind actions create larger displacement. Thus, GNSS based lateral displacement values are efficient in the measurement of the real structures.
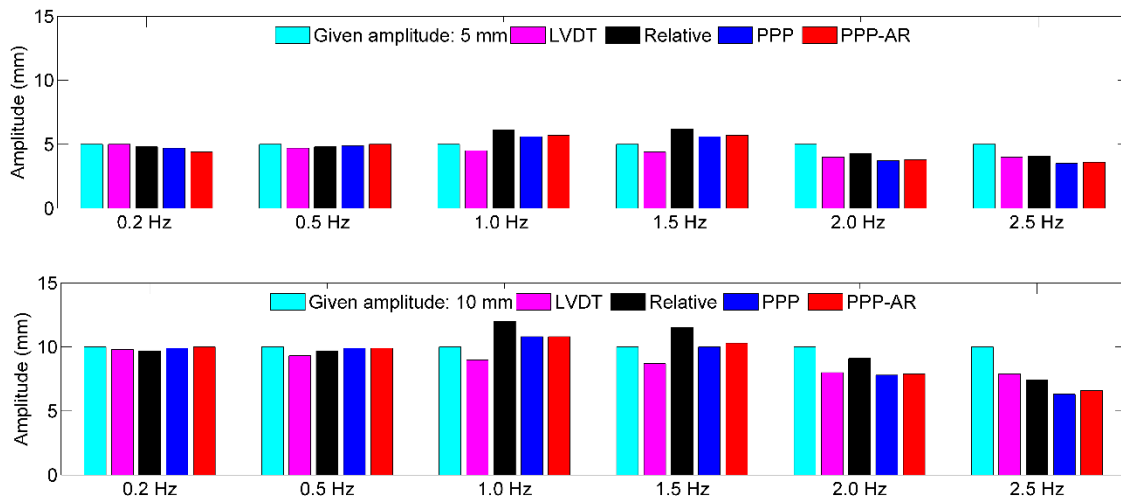

Fig. 9. The amplitude of peak frequency obtained from FFT for given 5- and 10-mm amplitude.

5.2 Results of the Kobe earthquake simulation test

Fig. 10 illustrates the time series of displacement caused by simulating a selected record of the Kobe earthquake. The Figure shows comparisons between the four discussed methods. It can be seen that the displacement waveforms estimated from PPP, PPP-AR, relative GNSS positioning and LVDT are largely consistent in terms of capturing the dynamic ground motion.
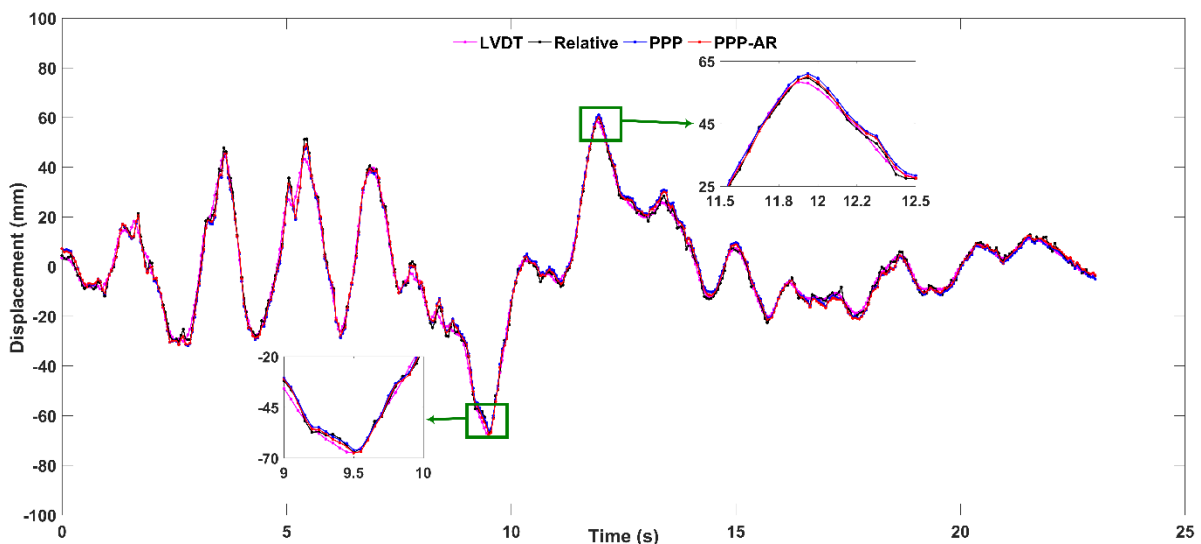
Fig. 10. Comparison among PPP, PPP-AR, relative GNSS positioning and LVDT-derived displacements at Kobe Earthquake simulation. LVDT data are down-sampled to 10 Hz.
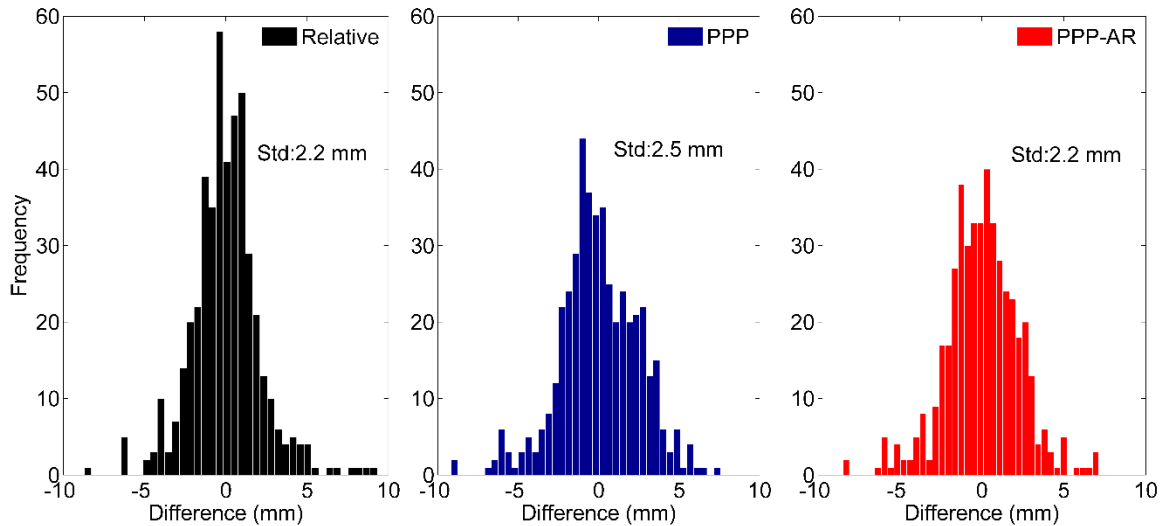
Fig. 11. Histograms of the differences between LVDT and each of the relative GNSS positioning, PPP, and PPP-AR displacements for the Kobe earthquake simulation

To further investigate the dynamic performance of PPP methods and relative positioning, the histogram of the differences in displacements between LVDT and each of the relative GNSS positioning, PPP, and PPP-AR are shown in Fig. 11. It is seen that the displacement waveforms from relative GNSS positioning, PPP and PPP-AR differ from those of the LVDT within -9 mm to 9 mm. The differences between PPP and LVDT are slightly larger than those between relative positioning, PPP-AR and LVDT, which indicates that the error level of relative positioning and PPP-AR is smaller than PPPduring the period of Kobe earthquake. This is expected outcome due to the fact that PPP is less accurate compared with relative positioning, where spatially correlated errors are practically eliminated in the relative positioning process, whereas some errors are estimated and some are externally provided in PPP algorithms, leaving some residual errors. When comparing PPP with PPP-AR, the standard deviation of the differences between PPP-AR and LVDT are slightly smaller than those between PPP and LVDT. This indicates that PPP-AR is more accurate than traditional float-ambiguity PPP during the period of the simulated earthquake (23 seconds).

In case of large earthquakes, Herring at al. (2018) show that relative positioning based on remote IGS sites, taken as reference stations, from earthquake epicenter can be used to resolve structural displacement response, using, for instance, GAMIT/TRACK software. However, it is not possible to detect natural vibration frequencies of the structures higher than 0.5 Hz with respect to the Nyquist theorem since the current sampling rate of GNSS data in global IGS network is 1 Hz, or even lower. Therefore, the use of high-rate PPP and PPP-AR (with high-rate orbit and clock correction products) represent an excellent approach to measure the absolute dynamic displacement of structures since PPP doesn't need any stable GNSS reference station(s) data like relative positioning methods.

5.3 Results of step motion tests

Fig. 12 shows a comparison for steps generated every 1 cm by the shaking table, from 1 cm to 5 cm. The comparison is performed between the three methods; i.e. relative positioning, PPP

and PPP-AR. The relative positioning solution was chosen to establish a reference trajectory for an accuracy assessment. As can be seen from Fig. 12, PPP and PPP-AR results are contaminated by long-period artifact, mainly due to multipath. However, as expected, PPP-AR results follow the relative solution more accurately than PPP results. The maximum difference between PPP-AR and relative positioning during 350 seconds is ~ 1.5 cm while the maximum difference between PPP and relative positioning is ~ 6.5 cm.
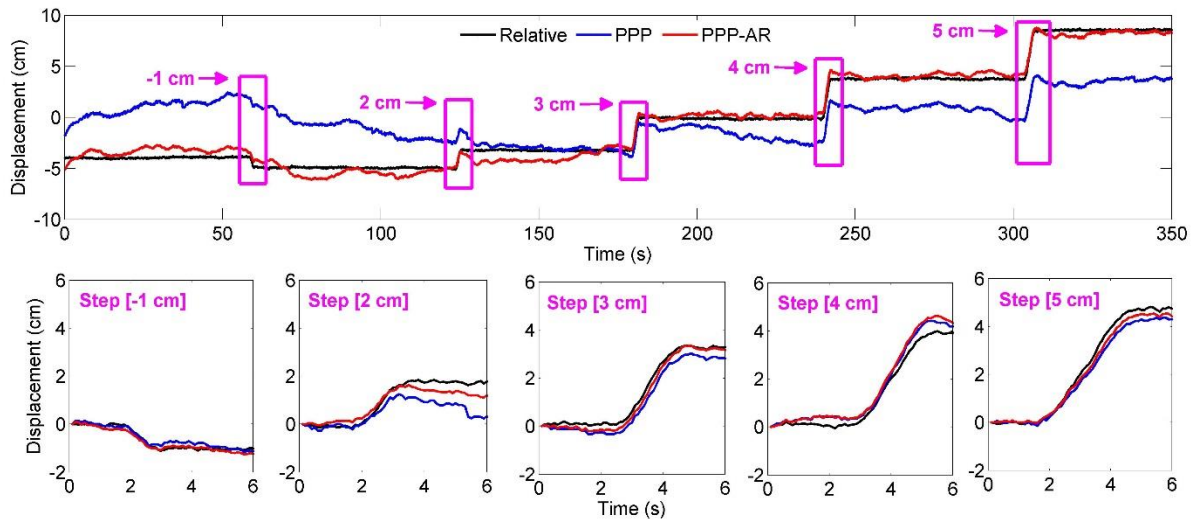
Fig. 12. Comparison of relative positioning, PPP and PPP-AR derived displacements at step function test.

Although there is still a long-period discrepancy between PPP and relative positioning, PPP can capture sudden changes within a short period of time. This result demonstrates that PPP-AR is much more accurate than PPP in terms of measuring quasi-static or static displacement offsets during a long period of time, indicating the superiority of the PPP-AR method for detecting quasi-static or static displacement offset. In other words, PPP-AR method is shown to be superior to the float PPP method if the investigated part of the time series increases over time.

5.4 Results of the small-scale model tests

In this subsection, the ability of PPP-AR method, as the most accurate PPP approach, to determine the natural frequencies of engineering structures under dynamic load was studied on a small-scale model (details were given in section 3.2 and Fig. 2). As seen in Fig. 13, the response time-series of the model under harmonic motions were computed from PPP-AR measurements of the two GNSS receivers mounted on the top of the model. The measurements were filtered with a moving average to remove the long-period components. The response of the engineering structures typically consists of 4 regions under the dynamic motions, namely static, transient, steady-state and free-vibration motions. If no lateral force acts on the structure, there would be a static-equilibrium under gravity forces, and when a dynamic force starts to act, the structure shifts from the static to a dynamic movement where the transient response occurs. Following a short-lasting transient motion, the steady-state response takes place, as long as the dynamic action exists. When the dynamic action diminishes, the structure, under no external excitation, starts the free-vibration motion for a time period depending on the inherent

damping. If the damping ratio is high, the free-vibration lasts for less time compared to the low damping-ratio case. In our tests, all the responses of the small-scale model excited by the shake-table are visible in the time series obtained from GNSS measurements, as depicted in Fig. 13. In this study, the free-vibration response of the model structure was studied since the structural characteristics are apparent in the decaying response.
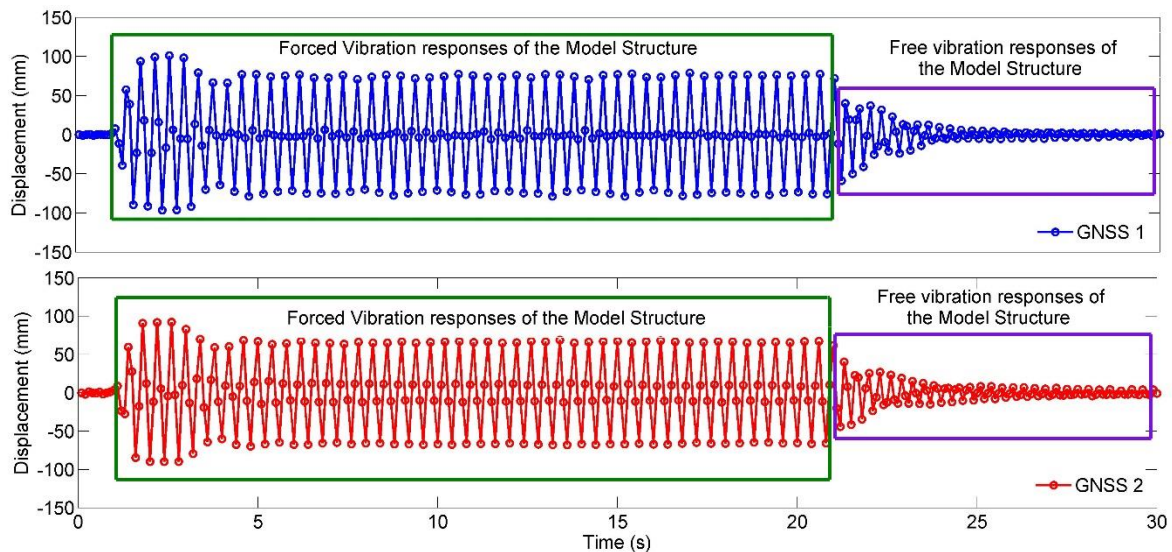

Fig. 13. Ground motion test: forced and free vibration responses of GNSS PPP-AR-derived time series after implementing moving average filter.

The FFT spectrums of the displacement time series of both receivers indicate identical spectral peak at 3.41 Hz with an amplitude of 1.8 mm and 2.8 mm, respectively, as shown in Fig. 14. The amplitude of the signal detected by GNSS receiver 2 (GNSS 2) is slightly larger than that of GNSS receiver 1 (GNSS 1), indicating that the model structure has a slight rotational motion other than perfect transition movement in the excitation direction. This is indeed the result of test setup strategy where GNSS 2 is not directly mounted on the top floor plate but to the tribrach. The additional mass of tribrach was intended to create an intentional torsional response of the structure. Hence, the additional mass on the GNSS 2 measurement point resulted in larger displacement compared to the displacement at the GNSS 1 measurement point.
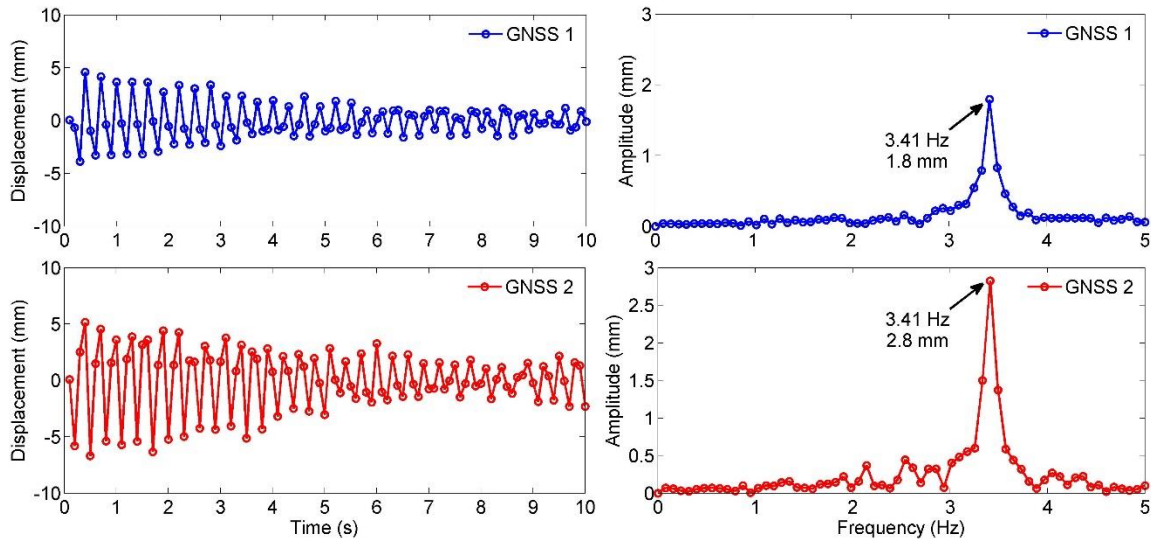
Fig. 14. Ground motion test: free vibration responses of GNSS PPP-AR-derived time series and FFT spectrum

The similar tendency in the amplitude difference of both observation points and the identical dominant vibration frequency is apparent in the FFT spectrum of the both GNSS measurements following a Hammer test, as shown in Fig.15 (Yigit et al. 2019).
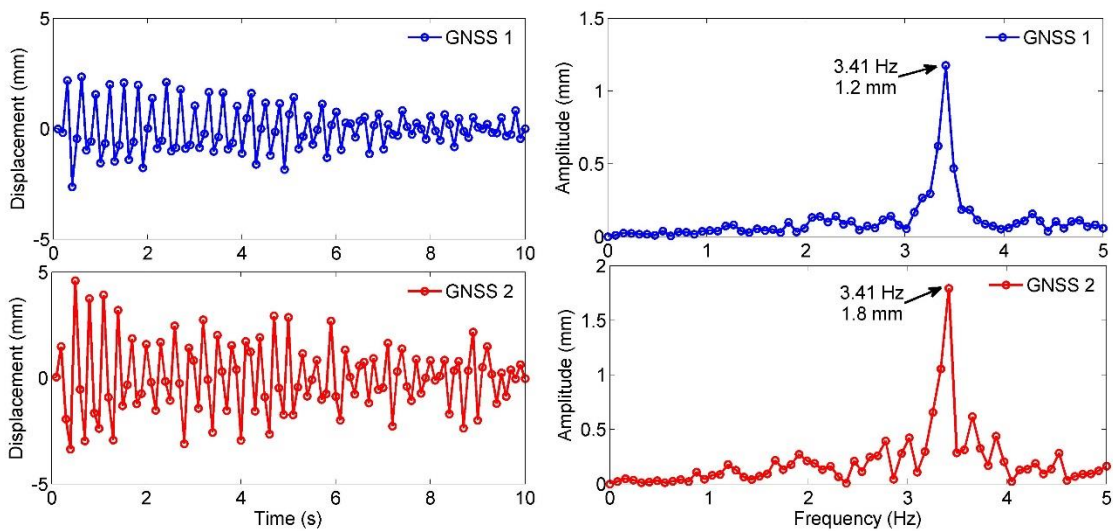
Fig. 15. Hammer Test: free vibration responses of GNSS PPP-AR-derived time series and FFT spectrum

The free-vibration amplitude of both time series is exponential, decaying in about 10 seconds. The measured natural frequency of the model structures shows a good agreement with that of FEM-derived natural frequency (see section 3.2). The Difference between PPP-AR-derived and FEM-derived natural frequencies is 0.08 Hz. This difference between the calculated and computed results can be attributed to the effect of uncertainties that cannot be included in the FEM analysis such as inherent damping and mass-distribution.

Since the sampling rate of GNSS receivers used in this study is 10 Hz, the first vibration mode of the small-scale structure could only be captured. According to the Nyquist theorem (Proakis and Manolakis, 1996), higher sampling frequency GNSS receivers (i.e. 20-, 50-, 100-Hz) are required to measure and detect the higher vibration modes of the model structure. Therefore, new tests using at least 20 Hz or higher sampling frequency GNSS receivers are needed to evaluate the ability of GNSS-PPP-AR.

6. Conclusion

In this study, various experiments using a shaking table were performed to test the ability of post-mission GNSS-PPP methods, both traditional PPP and PPP-AR, for measuring dynamic displacements, within a short period of time, and quasi-static/static displacement offset. The experiments included a harmonic oscillation experiment, Kobe earthquake simulation, quasi-static/static displacement offset, and a small-scale model experiment The performance of PPP and PPP-AR methods based on harmonic oscillation events and earthquake simulation has been assessed through a comparison with LVDT data output and relative GNSS positioning method in the time and frequency domains. The harmonic oscillation and earthquake experiments demonstrated good agreement among LVDT, the relative GNSS positioning, PPP and PPP-AR-derived spectrum. In general, the displacement waveforms estimated from the four methods are largely consistent in the dynamic component within a few millimeters. However, the step motion experiment demonstrated that PPP-AR method is more accurate than traditional PPP in detecting quasi-static/static displacement offset within both long and short period of time. Evaluation of the results reveals that there is no significant difference between PPP and PPP-AR for capturing dynamic movements within a short period of time, whereas the superiority of the PPP-AR method is apparent for capturing quasi-static or static displacement offset in case of a long period of time. In addition, small-scale model experiments showed that the high-rate PPP-AR method can precisely capture the frequencies of first motion mode of shear type structural response when compared with the FEM output. In conclusion, the PPP and PPP-AR methods are potentially good methods in determining the natural frequencies of engineering structures and form an acceptable substitute for relative positioning when the reference GNSS station data is unavailable or unreliable because of a large earthquake. The results of the experiments show that the PPP and PPP-AR method is efficient and can be applied for structural health monitoring (SHM) as well as relative positioning method in terms of measuring dynamic displacement and detecting natural frequencies of engineering structures.

Data Availability Statement

Some or all data, models, or code generated or used during the study are available from the corresponding author by request.

Acknowledgment

References

Akpınar, B., Dindar, A.A., Gurkan K.G., Gulal, V.E. and Aykut, N.O., 2017, "Establishment of National Network for Structural Health Monitoring (115Y250)", Research Report, TUBITAK 1005 Program.

Avallone, A, M. Marzario, A. Cirella, A. Piatanesi, A. Rovelli, C. Di Alessandro, E. D'Anastasio, N. D'Agostino, R. Giuliani, and M. Mattone. 2011. "Very high rate (10 Hz) GPS seismology for moderate-magnitude earthquakes: the case of the Mw 6.3 L'Aquila (central Italy) event" *J Geophys Res.* 116: 1–14. https://doi.org/10.1029/2010JB007834.

Bilich, A., J.F. Cassidy, and K.M. Larson. 2008. "GPS seismology: application to the 2002 Mw7.9 Denali fault earthquake" *Bull. Seismol. Soc. Am* 98:593–606. https://doi.org/10.1785/0120070096.

Bisnath, S., and Y. Gao. 2008. "Current State of Precise Point Positioning and Future Prospects and Limitations" International Association of Geodesy Symposia 133:615-623.

Bock, Y., D. Melgar, and B.W. Crowell. 2011. "Real-time strong-motion broadband displacements from collocated GPS and accelerometers" *Bull. Seismol. Soc. Am* 101:2904–2925. https://doi.org/10.1785/0120110007.

Breuer, P., T. Chmielewski, P. Gorski, E. Konopka, and L. Tarczynski. 2008. "The Stuttgart TV Tower - displacement of the top caused by the effects of sum and wind" *Eng Struct* 30:2771-81.

Calais, E., J.Y. Han, C. Demets, and J.M. Nocquet. 2006. "Deformation of the North American plate interior from a decade of continuous GPS measurements" *J Geophys Res* 111:1–23. https://doi.org/10.1029/2005JB004253.

Çelebi, M. 2000. "GPS in dynamic monitoring of long-period structures" *Soil Dyn Earthquake Eng* 20:477–483. https://doi.org/10.1016/S0267-7261(00)00094-4.

Chan, W.S., Y.L. Xu, X.L. Ding, Y.L. Xiong, and W.J. Dai. 2006. "Assessment of dynamic measurement accuracy of GPS in three directions" *J Surv Eng-ASCE* 132:108–117. https://doi.org/10.1061/(ASCE)0733-9453(2006)132:3(108).

Collins, P., S. Bisnath, L. Francois, and P. He´roux. 2010. "Undifferenced GPS ambiguity resolution using the decoupled clock model and ambiguity datum fixing" *Navigation* 57:123–135. https://doi.org/10.1002/j.2161-4296.2010.tb01772.x.

El-Mowafy, A. 2018. "Real-Time Precise Point Positioning Using Orbit and Clock Corrections as Quasi-Observations for Improved Detection of Faults" *J. of Navigation* 71:769-787. https://doi.org/10.1017/S0373463317001023.

El-Mowafy, A., M. Deo, and N. Kubo. 2017. "Maintaining real-time precise point positioning during outages of orbit and clock corrections" *GPS Solut.* 21:937-947. https://doi.org/10.1007/s10291-016-0583-4.

El-Mowafy, A, M. Deo, and C. Rizos. 2016. "On Biases in Precise Point Positioning with Multi-Constellation and Multi-Frequency GNSS Data" *Measurement Science and Technology* 27:035102. https://doi.org/10.1088/0957-0233/27/3/035102.

Ge, L., S. Han, C. Rizos, Y. Ishikawa, M. Hoshiba, and Y. Yoshida. 2000. "GPS seismometers with up to 20 Hz sampling rate" *Earth Planets Space* 58:881–884. https://doi.org/10.1186/BF03352300.

Ge, M., G. Gendt, M. Rothacher, C. Shi, and J. Liu. 2008. "Resolution of GPS Carrier-Phase Ambiguities in Precise Point Positioning (PPP) with Daily Observations" *Journal of Geodesy* 82:389–399. https://doi.org/10.1007/s00190-007-0187-4.

Górski, P. 2017. "Dynamic characteristic of tall industrial chimney estimated from GPS measurement and frequency domain decomposition" *Eng Struct* 148:277–292. https://doi.org/10.1016/j.engstruct.2017.06.066.

Herring, T., C. Gu, M.N. Toksöz, J. Parol, F. Al-jeri, J. Al-qazweeni, H. Kamal, and O. Büyüköztürk. 2018. "GPS Measured Response of a Tall Building due to a Distant M w 7.3 Earthquake" *Seismological Research Letters* 90:149-159. https://doi.org/10.1785/0220180147.

Hung, H.K., and R.J. Rau. 2013. "Surfacewaves of the 2011 Tohoku earthquake: Observations of Taiwan's dense high-rate GPS network" *J. Geophys. Res* 118:332–345. https://doi.org/10.1029/2012JB009689.

Kaloop, M.R., C.O. Yigit, and J.H. Hu. 2018. "Analysis of the dynamic behavior of structures using the high-rate GNSS-PPP method combined with a wavelet-neural model: Numerical simulation and experimental tests" *Adv. Space Res* 61:1512-1524. https://doi.org/10.1016/j.asr.2018.01.005.

Kouba, J. 2003. "Measuring seismic waves induced by large earthquakes with GPS" *Stud Geophys Geod* 47:741–755. https://doi.org/10.1023/A:1026390618355.

Kouba, J., and P. Hérou. 2001. "Precise Point Positioning using IGS orbit and clock products" *GPS Solut.* 5:12–28. https://doi.org/10.1007/PL00012883.

Laurichesse, D., F. Mercier, J. Berthias, and J. Bijac. 2008. "Real time zero difference ambiguities blocking and absolute RTK" In: Proceedings of the ION NTM-2008, Institute of Navigation, San Diego, California, Jan 2008 747–755

Li, X, L. Ge, E. Ambikairajah, C. Rizos, Y. Tamura, and A. Yoshida. 2006. "Full-scale structural monitoring using an integrated GPS and accelerometer system" *GPS Solutions* 10:233–247. https://doi.org/10.1007/s10291-006-0023-y.

Li, X., M. Ge, X. Zhang, Y. Zhang, B. Guo, R. Wang, J. Klotz, and J. Wickert. 2013. "Real-time high-rate co-seismic displacement from ambiguity-fixed Precise Point Positioning: application to earthquake early warning" *Geophys Res Lett* 40:295–300. https://doi.org/10.1002/grl.50138.

Meng, X., A.H. Dodson, and G.W. Roberts. 2007. "Detecting bridge dynamics with GPS and triaxial accelerometers" *Eng Struct* 29:3178–3184. https://doi.org/10.1016/j.engstruct.2007.03.012.

Mireault, Y., P. Tétreault , F. Lahaye , P. Héroux , and J. Kouba. 2008. "Online precise point positioning: a new, timely service from natural resources Canada" *GPS World* 19:53 64.

Moschas, F., A. Avallone, V. Saltogianni, and S.C. Stiros. 2014. "Strong motion displacement waveforms using 10-Hz precise point positioning GPS: an assessment based on free oscillation experiments" *Earthquake Eng Struct Dyn* 43:1853–1866. https://doi.org/10.1002/eqe.2426.

Moschas, F., and S. Stiros. 2011. "Measurement of the dynamic displacements and of the modal frequencies of a short-span pedestrian bridge using GPS and an accelerometer" *Eng Struct* 33:10–7. http://dx.doi.org/10.1016/j.engstruct.2010.09.013.

Nickitopoulou, A., K. Protopsalti, and S.C. Stiros. 2006. "Monitoring dynamic and quasi-static deformations of large flexible engineering structures with GPS: accuracy, limitations and promises" *Eng Struct* 28:1471–82. https://doi.org/10.1016/j.engstruct.2006.02.001.

Nie, Z., R. Zhang, G. Liu, Z. Jia, D. Wang, Y. Zhou, and M. Lin. 2016. "GNSS seismometer: Seismic phase recognition of real-time high-rate GNSS deformation waves" *Journal of Applied Geophysics* 135:328–337. https://doi.org/10.1016/j.jappgeo.2016.10.026.

Park, H.S., H.G. Sohn, I.S. Kim, and J.H. Park. 2008. "Application of GPS to monitoring of wind-induced responses of high-rise buildings" *Struct Des Tall Spec Build* 17:117–132. https://doi.org/10.1002/tal.335.

Paziewski, J., R. Sieradzki, and R. Baryla. 2018. "Multi-GNSS high-rate RTK, PPP and novel direct phase observation processing method: application to precise dynamic displacement detection" *Measurement Science and Technology* 29:035002. https://doi.org/10.1088/1361-6501/aa9ec2.

Proakis J.G., and D.G. Manolakis. 1996. *Digital signal processing: Principles, algorithms and applications*. 3rd ed. New Jersey, USA: Prentice Hall International.

Psimoulis, P.A., and S.C. Stiros. 2008. "Experimental assessment of the accuracy of GPS and RTS for the determination of the parameters of oscillation of major structures" *Comput-Aided Civil Infrastructure Eng* 23:389–403. https://doi.org/10.1111/j.1467-8667.2008.00547.x.

Roberts, G.W., X. Meng, and A. Dodson. 2004. "Integrating a global positioning system and accelerometers to monitor deflection of bridges" *J Surv Eng.-ASCE* 130:65–72. https://doi.org/10.1061/(ASCE)0733-9453(2004)130:2(65).

Savage, J.C., W. Gan, W.H. Prescott, and J.L. Svarc. 2004. "Strain accumulation across the coast ranges at the latitude of San Francisco, 1994–2000" *J Geophys Res.* 109:1–11. https://doi.org/10.1029/2003JB002612.

Shi, C., Y. Lou, H. Zhang, Q. Zhao, J. Geng, R. Wang, R. Fang, and J. Liu. 2010. "Seismic deformation of the Mw8.0 Wenchuan earthquake from high-rate GPS observations" *Adv. Space Res* 46:228–235. https://doi.org/10.1016/j.geog.2016.04.009.

Shu, Y., Y. Shi, P. Xu, X. Niu, J. Liu. 2017. "Error analysis of high-rate GNSS precise point positioning for seismic wave measurement" *Adv. Space Res* 59:2691–2713. https://doi.org/10.1016/j.asr.2017.02.006.

Tang, X., G.W. Roberts, X. Li, and C. Hancock. 2017. "Real-time kinematicPPP GPS for structure monitoring applied on the Severn suspension bridge, UK" *Adv. Space Res* 60:925–937. https://doi.org/10.1016/j.asr.2017.05.010.

Tétreault, P., J. Kouba, P. Héroux, and P. Legree. 2005. "CSRS-PPP: an internet service for GPS user access to the Canadian spatial reference frame" *Geomatica* 59:17–28.

Tu, R., R. Wang, M. Ge, T. R. Walter, M. Ramatschi, C. Milkereit, D. Bindi, and T. Dahm. 2013. "Cost-effective monitoring of ground motion related to earthquakes, landslides, or volcanic activity by joint use of a single-frequency GPS and a MEMS accelerometer" Geophys Res Lett 40:3825-3829. https://doi.org/10.1002/grl.50653

Tu, R., M. Ge, R. Wang, and T.R. Walter. 2014. "A new algorithm for tight integration of real-time GPS and strong-motion records demonstrated on simulated, experimental, and real seismic data" J Seismol 18:151-161. https://doi.org/10.1007/s10950-013-9408-x

Wang, G., F. Blume, C. Meertens, P. Ibanez, and M. Schulze. 2011. "Performance of high-rate kinematic GPS during strong shaking: observations from shaking table tests and the 2010 Chile earthquake" *J Geodetic Sci* 2:1–15. https://doi.org/10.1186/BF03352300.

Xu, P., C. Shi, R. Fang, J. Liu, X. Niu, Q. Zhang, and T. Yanagidani. 2013. "High-rate precise point positioning (PPP) to measure seismic wave motions: an experimental comparison of GPS PPP with inertial measurement units" *J Geod* 87:361–372. https://doi.org/10.1007/s00190-012-0606-z.

Xu, P., Y. Shu, X. Niu, W. Yao, and Q. Chen. 2019. "High-rate multi-GNSS attitude determination: experiments, comparisons with inertial measurement units and applications of GNSS rotational seismology to the 2011 Tohoku Mw9.0 earthquake" *Measurement Science and Technology* 30:024003. https://doi.org/10.1088/1361-6501/aaf987.

Xu, Y., J.M.W. Brownjohn, D. Hester, and K.Y. Koo 2017. "Long-span bridges: Enhanced data fusion of GPS displacement and deck accelerations" *Eng Struct* 147:639–651. https://doi.org/10.1016/j.engstruct.2017.06.018.

Yigit, C.O. 2016. "Experimental assessment of post processed kinematic precise point positioning method for structural health monitoring" *Geomat Nat Hazards Risk* 7:363–380. https://doi.org/10.1080/19475705.2014.917724.

Yigit, C.O., and E. Gurlek. 2017. "Experimental testing of high-rate GNSS precise point positioning (PPP) method for detecting dynamic vertical displacement response of engineering structures" *Geomat., Nat. Haz. Risk* 8:893-904. https://doi.org/10.1080/19475705.2017.1284160.

Yigit, C.O., X. Li, C. Inal, L. Ge, and M. Yetkin. 2010. "Preliminary evaluation of precise inclination sensor and GPS for monitoring full-scale dynamic response of a tall reinforced concrete building" *J Appl Geod* 4:103–113. https://doi.org/10.1515/jag.2010.010.

Yigit, C.O., A.A. Dindar, A. El-Mowafy, M. Bezcioglu, and V. Gikas. 2019 "Investigating the ability of high-rate GNSS-PPP for determining the vibration modes of engineering structures: small scale model experiment." *4th Joint International Symposium on Deformation Monitoring*, 15-17 May 2019, Athens, Greece.

Zumberge, J.F., M.B. Heflin, D.C. Jefferson, M.M. Watkins, and F.H. Webb. 1997. "Precise Point Positioning for the efficient and robust analysis of GPS data from large networks" *J Geophys Res* 102:5005–5017. https://doi.org/10.1029/96JB03860.